Bull Math Biol (2014) 76:2884–2906
DOI 10.1007/s11538-014-0037-5

Society for Mathematical Biology

ORIGINAL ARTICLE

A Validated Mathematical Model of Tumor Growth Including Tumor–Host Interaction, Cell-Mediated Immune Response and Chemotherapy

Álvaro G. López · Jesús M. Seoane · Miguel A. F. Sanjuán

Received: 13 June 2014 / Accepted: 2 October 2014 / Published online: 28 October 2014

Abstract We consider a dynamical model of cancer growth including three interacting cell populations of tumor cells, healthy host cells and immune effector cells. The tumor–immune and the tumor–host interactions are characterized to reproduce experimental results. A thorough dynamical analysis of the model is carried out, showing its capability to explain theoretical and empirical knowledge about tumor development. A chemotherapy treatment reproducing different experiments is also introduced. We believe that this simple model can serve as a foundation for the development of more complicated and specific cancer models.

Keywords Cancer dynamics · Immune cells · Mathematical modeling

1 Introduction

It is increasingly apparent that the growth deregulation within a tumor can only be explained once we understand the contributions of the host healthy cells present with it, which play key roles in driving tumor cell proliferation. Signaling interactions between the stromal and the neoplastic tissue may ultimately prove to be as important as the cancer cell autonomous mechanisms in explaining tumor cell proliferation (Hanahan and Weinberg 2000). The importance of the immune system fighting the growth of tumors is undeniable, to the point that immunotherapy is lately focusing major attention of cancer therapists and researchers (Couzin-Frankel 2013). Also chemotherapy treatments are under constant examination, in the pursuit of better distribution mechanisms that diminish the toxicity of the anticancer drugs (Pastorino et al. 2006), as

Á. G. López · J. M. Seoane · M. A. F. Sanjuán (✉)
Nonlinear Dynamics, Chaos and Complex Systems Group, Departamento de Física, Universidad Rey Juan Carlos, Tulipán s/n, 28933 Móstoles, Madrid, Spain
e-mail: miguel.sanjuan@urjc.es

well as protocols that evade the resistance of tumor cells to such cytotoxic substances (Lavi et al. 2012). Mathematical modeling of tumor growth (Bellomo et al. 2008) has been widely used to explain different aspects of tumor progression, such as tumor dormancy, sneaking through, angiogenic switch, invasion, morphology. Therefore, the development of validated and simple mathematical models representing several types of tissues and the nonlinear interactions among them, as well as therapy protocols, is of paramount importance.

The main goal of the present work was to develop a validated ODE model of tumor progression with three interacting cell populations representing the healthy tissue, the neoplastic tissue and the immune effector cells. For this purpose, we derive the dynamical system equations from a similar validated model describing immune and tumor dynamics (De Pillis et al. 2005), but that considers different cell populations for innate and specific immune responses and disregards tumor–host interplay. Here, the immune response is integrated in a single cell population, as it was the case of older models (De Pillis and Radunskaya 2003), allowing us to include a population representing the healthy tissue and still to visualize in a simple manner their dynamical phase space. By means of the least-squares fitting method, we adjust the model to experimental data (Diefenbach et al. 2001), verifying that the lysis of cancer cells by the effector constituents of the immune system is accurately reproduced by the model. As a completely new feature regarding previous modeling of this nature, we also introduce a chemotherapy protocol validated with in vivo experiments in mice (Hiramoto and Ghanta 1974). To reproduce the time evolution of the experimental fractional tumor cell kill by the chemotherapeutic agents, a new method is proposed that avoids dealing with complex pharmacokinetical models. The study is closed with the examination of correlations between the model and the experiments.

2 Model Development

All the biological assumptions considered to set up the model equations are based on both accepted knowledge of basic laws governing tumor growth and the immune system function (De Pillis et al. 2005; Diefenbach et al. 2001; Kuznetsov et al. 1994). The tumor–host competition for space and resources is developed following previous modeling (De Pillis and Radunskaya 2003; Gatenby and Gawlinsky 1996; Kirschner and Panetta 1988; Pinho et al. 2002), while the law governing the fractional tumor cell kill of by the chemotherapeutic drugs is derived from the exponential kill model (Gardner 1996), developed in accordance with in vitro experiments.

The growth of the cell populations is assumed to be logistic for both the tumor T and the healthy cells H, with growth rates r_1 and r_2, and carrying capacities K_1 and K_2. Other types of laws, such as Gompertz law, have no relevant consequences in the dynamics and might be used as well. We use ordinary competition terms frequently appearing in Lotka–Volterra models, identical to those used in De Pillis and Radunskaya (2003) and Gatenby and Gawlinsky (1996). Finally, the immune response and the destruction of the neoplastic tissue are built up from the one presented in De Pillis et al. (2005), which was validated with data from published mouse (Diefenbach et al. 2001) and human (Dudley et al. 2002) studies. The model of cell-mediated immune

response described in that work consists of a tumor cell population T interacting with two immune cell populations, the natural killers N and the CD8$^+$ T lymphocytes L. The fractional tumor cell kill by T cells is given by a Hill function $D(L,T)$ depending on L/T, while the fractional tumor cell kill by NK cells is proportional to the number of such cells. The NK cells dynamics is modeled with four terms: a constant input σ responsible for innate immunity, a recruitment contribution $gT^2/(h+T^2)N$, a competition term pNT with tumor cells and a decay term representing the death fN of the natural killers, which after several interactions with the tumor cells become inactivated. The CTLs dynamics is governed by analogous laws, but there is no constant input of cells, since they correspond to acquired immunity. On the other hand, it includes the stimulation of T lymphocytes in response to the interaction between NK and tumor cells rTN. The activation term is $jD^2T^2/(k+D^2T^2)L$, the death term is mL and the competition one is qLT.

It can be numerically shown that for many initial conditions and not long times, these two immune cell populations are more or less related in a linear fashion. In this manner, we identify them and linearly combine their equations, simply referring to them as effector cells E. The resulting model is as follows

$$\begin{aligned}
\dot{T} &= r_1 T\left(1-\frac{T}{K_1}\right) - a_{12}HT - a_{13}ET - D(E,T)T \\
\dot{H} &= r_2 H\left(1-\frac{H}{K_2}\right) - a_{21}TH \\
\dot{E} &= \sigma - d_3 E + \tilde{g}\frac{T^2}{\tilde{h}+T^2}E + g\frac{D^2(E,T)T^2}{h+D^2(E,T)T^2}E - a_{31}TE,
\end{aligned} \tag{1}$$

with

$$D(E,T) = d\frac{(E/T)^\lambda}{s+(E/T)^\lambda}. \tag{2}$$

This fractional cell kill law was a novel feature discovered and introduced in De Pillis et al. (2005), so deserves some comments. To give some hints on the significance and possible explanations of this law, we rewrite it in the following form

$$D(E,T) = d\frac{E^\lambda}{sT^\lambda + E^\lambda}. \tag{3}$$

Written this way, the law states that the more effector cells, the greater the fractional cell kill, but bearing in mind the saturation of antigen-mediated immune response, which depends on the tumor load. The value for which the fraction cell kill is half of its maximum is given by $E_{hm} = s^{1/\lambda}T$, what means that bigger tumors are harder to fight by T lymphocytes. If two tumors of the same nature and different size at a certain time instant are lysed at the same rate by the immune system, the bigger tumor will require more effector cells. This is because an immune cell destroys tumor cells one by one, and the number of encounters is limited by the inactivation of the effector cells.

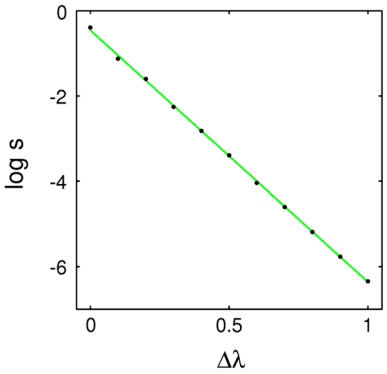

Fig. 1 Changes in the parameter s required to validate the model when the parameter λ in the function $h(T) = sT^{\lambda}$ is changed to $\lambda + \Delta\lambda$. The case $\Delta\lambda = 0$ corresponds to the (ll) values shown in Table 1. The relation is explained by the level curves of the function sT^{λ} in the parameter space (λ, s), which can be expressed in the form $\log s = \log c(T) - \lambda \log T$. Averaging this equation in time, we obtain the equation $\log s = a - b\lambda$. A linear regression has been performed to confirm the previous assertion, obtaining the relation $\log s = -0.46 - 5.79\Delta\lambda$, with a coefficient of determination $R^2 = 0.9996$

Or equivalently, if two tumors of different size are reduced to a particular fraction of its size after a certain period of time, the bigger tumor will require more effector cells. On the other hand, in our opinion, the saturation effect in this law might be tacitly including geometrical properties of the tumor and their consequences (e.g., crowding effects and accessibility of the immune cells). We believe that it would be desirable to propose a general law of the form

$$D(E, T) = d\frac{E^{\lambda}}{h(T) + E^{\lambda}}, \tag{4}$$

and study different functions depending on the tumor load $h(T)$ for different tumors. In the cited work, $h(T) = sT^{\lambda}$ is used. We have tested the importance of the parameter λ by studying deviations from this function in the form $h(T) = sT^{\lambda+\Delta\lambda}$, and we have found that shifts $\Delta\lambda/\lambda$ even higher than one are still capable of validating in an accurate manner the immune response by simply decreasing the value of the parameter s. The precise relation between $\Delta\lambda$ and s is depicted in Fig. 1, and it is explained by noting that the function $h(T)$ can be thought as a surface in the parameter space (λ, s), so that changes in the parameters along a level curve $sT^{\lambda} = c(T)$ are also capable of validating the experimental results. This means that the rational form E/T appearing in (2) may not generally hold and cannot be derived solely from the experiments used in De Pillis et al. (2005). What can be safely deduced from such experiments is that $h(T)$ increases with the tumor size. Therefore, the dePillis–Radunskaya–Wiseman law (PRW law) states that the number of the T cells for which the fractional tumor cell kill is half of its maximum, increases monotonically with the tumor burden. It remains unexplained why the same does not happen for the NK cells as well. As pointed out in De Pillis et al. (2005), this might be due to the fact that NK cells are less effective destroying tumor cells. Generally, a T lymphocyte is able to destroy more tumor cells

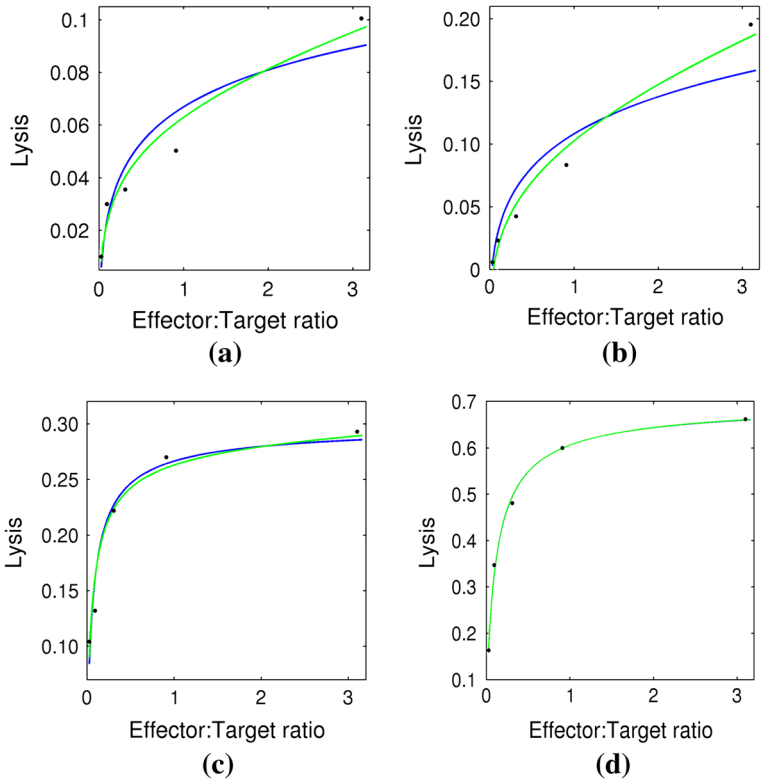

Fig. 2 Data and the predicted curves from the models for the lysis of tumor cells by the effector cells. The green curve represents the general model, while the blue corresponds to its simplified version. **a** The experiment where the effector cells are primary challenged with ligand-negative-transduced cells and then rechallenged again with control-transduced cells (nn). **b** The case for which the effector cells are primary challenged with ligand-negative-transduced cells and then rechallenged with ligand-transduced cells (nl). **c** In this case, the effector cells are primary challenged with ligand-transduced cells and then rechallenged with control-transduced cells (ln). **d** The experiment where the effector cells are primary challenged with ligand-transduced cells and then rechallenged again with ligand-transduced cells (ll)

during its life cycle than a natural killer cell (Mallet and De Pillis 2006). Note also that to obtain similar values for the lysis of tumor cells by T cells and NK cells, much higher values of the effector:target ratio are required for the last (De Pillis et al. 2005). This hypothesis is also supported by the fact that the PRW law fits better the experimental results for which the immune system is more effective, as can be seen in Fig. 2.

The model shown above fits the data accurately, but it is quite hard to manage when investigating its dynamical properties. A simplified version of this model capable of reproducing experimental data can be obtained by neglecting the recruitment and lysis of the NK cells, which are more ineffective fighting the tumor cells. Note, however, that the role of the NK cells is indirectly present in the model, in the background source rate σ. The equations are now

$$\begin{aligned}
\dot{T} &= r_1 T\left(1-\frac{T}{K_1}\right) - a_{12}HT - D(E,T)T \\
\dot{H} &= r_2 H\left(1-\frac{H}{K_2}\right) - a_{21}TH \\
\dot{E} &= \sigma - d_3 E + g\frac{D^2(E,T)T^2}{h+D^2(E,T)T^2}E - a_{31}TE.
\end{aligned} \tag{5}$$

The chemotherapy treatment is here described by the exponential kill model, which proposes the fractional cell kill law $k_i(C) = b_i(1-e^{-\rho_i C})$, with $i = 1, 2, 3$ and C the drug concentration at the tumor site, which dynamics is given by a single compartment model and first-order pharmacokinetics. Therefore, the whole set of equations reads

$$\begin{aligned}
\dot{T} &= r_1 T\left(1-\frac{T}{K_1}\right) - a_{12}HT - D(E,T)T - k_1(C)T \\
\dot{H} &= r_2 H\left(1-\frac{H}{K_2}\right) - a_{21}TH - k_2(C)H \\
\dot{E} &= \sigma - d_3 E + g\frac{D^2(E,T)T^2}{h+D^2(E,T)T^2}E - a_{31}TE - k_3(C)E \\
\dot{C} &= I(t) - k_e C,
\end{aligned} \tag{6}$$

with $I(t)$ the input of drug and k_e the rate of elimination of the drug from the body. In fact, to reproduce in vivo experiments, the fractional cell kill law $k(C)$ is modeled depending on the time-delayed concentration of drug $C(t-\tau)$.

Finally, the cooperation between the healthy and the tumor tissues is not modeled here. The reason is that the paracrine signals stimulating tumor growth come from ancillary cells (e.g., fibroblasts), different from the host cells (e.g., epithelial cells) from which the tumor evolves (Olumi et al. 1999). Moreover, the stromal cells cooperating with the tumor differ from the normal stromal cells. Therefore, a model with several healthy cell populations representing the different types of tissues should be considered to rigorously represent the tumor microenvironment.

3 Fitting the Model to Experimental Data

We fit both, the model and its simplified version, to four experimental situations, proving that the tumor–immune interaction is again validated with accuracy. The data used to arrange the equations and fix the parameters of our mathematical model are obtained from Diefenbach et al. (2001). In this work, the authors study the effects of ectopically expressing NKG2D ligands in three tumor cell lines, which resulted in the rejection of the tumors by syngeneic B6 mice. Such rejection was mediated by NK cells and $CD8^+$ T cells. Their experimental results demonstrate that a high enough expression of these ligands creates a significant barrier to the tumor establishment in mice. In particular, the data borrowed from this work and used to fit the model correspond to the point where the authors address whether prior immunization with tumor cells that express ligands of the NKG2D receptor induces protective immunity

to ligand-negative tumor cells. The NK and $CD8^+$ T cells lysis of a T-cell lymphoma after primary challenging with ligand-expressed cell transductants and being again challenged with ligand-transduced or ligand-negative-transduced cells is reported. More specifically, we deal with four possible scenarios: a primary challenge with control-transduced cells followed by a secondary challenge with ligand or control cells, and a primary interaction with ligand-transduced cells followed again by ligand or ligand-negative rechallenges.

Firstly, we give a summary of the parameters used, which are listed in Tables 1 and 2, together with the corresponding sources in which the parameter estimation methods are explained. As in Gatenby and Gawlinsky (1996), we consider similar carrying capacities K_i for the tumor and the healthy tissue, assuming that generally the tumor occupies a region that otherwise would be filled with normal cells. Also the rates of growth r_i of both cell populations take very close values, following the same reference, but we assume that the tumor grows faster in the absence of competition and immune surveillance, since its dependence on cell to cell signaling for growth is smaller (Hanahan and Weinberg 2000). These four parameters, the recruitment rates and steepnesses, the constant input, as well as the inactivation rate of the effector cells, are borrowed from Refs. 6 and 10. It has been demonstrated that the Gompertz law of growth of tumor cell populations is a robust emergent feature of cancer dynamics under nutrient competition among tumor cells (Ferreira et al. 2002). It is commonly considered (De Pillis and Radunskaya 2003) that the competition between the neoplastic and the healthy tissues is indirect, what means that cells do not kill each other, but struggle for territory and nutrient resources. However, a very important source of competition between the tumor and the healthy host cells is due to the acidic environment in which tumor cells develop, which is a consequence of the primitive metabolic pathways they use (Gatenby and Gawlinsky 1996; Warburg 1956; Van der Heiden et al. 2009). In fact, if we neglect spatial dependence in the equation governing the excess of H^+ ions in the model presented in Gatenby and Gawlinsky (1996), the stationary state gives a fixed point for ion concentration proportional to the number of tumor cells. Clearly stated, the more the tumor cells, the lower the pH and the worse for the healthy tissue. When substituted in the reaction–diffusion equation governing the dynamics of the healthy host cells, we obtain another competition term between the host and the tumor cells. Therefore, we assume that the tumor cells compete in a more aggressive manner and set $a_{12} < a_{21}$. The effects of changing these parameters are reported in Sect. 4, and rough estimates are provided in Sect. 6.

According to the experiments taken from Diefenbach et al. (2001), the model validation should be carried out in two separate steps, one for each type of effector cells. For instance, the first could involve the validation of the results concerning NK cells to obtain the value of the parameter a_{13} for the ligand and ligand-negative-transduced cells. Then, after setting a_{13} to zero, the experimental lysis of $CD8^+$ T cells should be fitted for the different cases. Finally, both contributions would be added to the model. However, another possibility is to fit only CTLs results and let the parameter a_{13} take diverse values. This procedure allows more accurate fittings and has the advantage of suggesting a generalization of the PRW law, as explained at the end of the present section. To avoid the risks of overfitting because of using too many parameters, we have to proceed carefully. Since the model is derived from an original validated model, we

Table 1 Values of the parameters used to compute the curves representing the lysis of cancer cells by the effector cells, for the general model given by (1)

Parameter	Units	Value	Description	Source
r_1	day^{-1}	5.14×10^{-1}	Tumor cells growth rate	(6)
K_1	cell	9.8×10^{8}	Tumor carrying capacity	(6)
a_{12}	$\text{cell}^{-1}\ \text{day}^{-1}$	1.1×10^{-10}	Competition of host cells with tumor cells	
$a_{13}(nn)$	$\text{cell}^{-1}\ \text{day}^{-1}$	5.2×10^{-8}	Fractional tumor cell kill of the power law	(6)
$a_{13}(nl)$		1.6×10^{-7}		(6)
$a_{13}(ln)$		3.2×10^{-8}		(6)
$a_{13}(ll)$		8.5×10^{-9}		(6)
$d(nn)$	day^{-1}	2.20	Saturation level of fractional tumor cell kill of the PRW law	
$d(nl)$		3.47		
$d(ln)$		2.60		
$d(ll)$		7.86		
$s(nn)$	None	1.6	Steepness coefficient of the PRW law	
$s(nl)$		2.5		
$s(ln)$		1.4×10^{-1}		
$s(ll)$		4.0×10^{-1}		
$\lambda(nn)$	None	1.2×10^{-1}	Exponent of the PRW law	
$\lambda(nl)$		2.1×10^{-1}		
$\lambda(ln)$		7.0×10^{-1}		
$\lambda(ll)$		7.0×10^{-1}		
r_2	day^{-1}	1.80×10^{-1}	Host cells growth rate	(6, 11)
K_2	cell	1.0×10^{9}	Host cells carrying capacity	(6, 11)
a_{21}	$\text{cell}^{-1}\ \text{day}^{-1}$	4.8×10^{-10}	Competition of tumor cells with host cells	
σ	cells day^{-1}	7.5×10^{4}	Constant source of effector cells	(10)
d_3	day^{-1}	6.12×10^{-2}	Inactivation rate of effector cells	(6)
$\tilde{g}(n)$	day^{-1}	2.5×10^{-2}	Maximum recruitment rate related to the power law	(6)
$\tilde{g}(l)$		2.0×10^{-1}		(6)
$g(nn)$	day^{-1}	3.75×10^{-2}	Maximum recruitment rate related to the PRW law	(6)
$g(nl)$		3.75×10^{-2}		(6)
$g(ln)$		1.13×10^{-1}		(6)
$g(ll)$		3.00×10^{-1}		(6)
$\tilde{h}$	cell^{2}	2.02×10^{7}	Steepness coefficient for recruitment related to the power law	(10)

Table 1 continued

Parameter	Units	Value	Description	Source
h	cell^2	2.02×10^7	Steepness coefficient for the recruitment related to the PRW law	(10)
a_{31}	cell $^{-1}$ day $^{-1}$	2.8×10^{-9}	Immune–tumor competition	(10)

The parameters of the PRW law, λ and d, are obtained by a least-squares fitting of the solutions of the system of differential equations to the experimental data. The parenthesis represents four different cases: a primary challenge with control-transduced cells followed by a secondary one with ligand (nl) or control (nn) cells, and a primary interaction with ligand-transduced cells followed again by ligand (ll) or ligand-negative (ln) rechallenges

Table 2 Values of the parameters used to compute the curves representing the lysis of cancer cells by the effector cells, for the simplified model given by (5)

Parameter	Units	Value	Description	Source
r_1	day^{-1}	5.14×10^{-1}	Tumor cells growth rate	(6)
K_1	cell	9.8×10^8	Tumor carrying capacity	(6)
a_{12}	cell $^{-1}$ day $^{-1}$	1.1×10^{-10}	Competition of host cells with tumor cells	
$d(nn)$	day^{-1}	2.6	Saturation level of fractional tumor cell kill of the PRW law	
$d(nl)$		7.1		
$d(ln)$		2.7		
$d(ll)$		7.9		
$s(nn)$	None	1.8	Steepness coefficient of the PRW law	
$s(nl)$		5.0		
$s(ln)$		1.4×10^{-1}		
$s(ll)$		4.0×10^{-1}		
$\lambda(nn)$	None	2.2×10^{-1}	Exponent of the PRW law	
$\lambda(nl)$		2.5×10^{-1}		
$\lambda(ln)$		7.3×10^{-1}		
$\lambda(ll)$		7.0×10^{-1}		
r_2	day^{-1}	1.80×10^{-1}	Host cells growth rate	(6, 11)
K_2	cell	1.0×10^9	Host cells carrying capacity	(6, 11)
a_{21}	cell $^{-1}$ day $^{-1}$	4.8×10^{-10}	Competition of tumor cells with host cells	
σ	cells day^{-1}	7.5×10^4	Constant source of effector cells	(10)
d_3	day^{-1}	6.12×10^{-2}	Death of effector cells	(6)
$g(nn)$	day^{-1}	3.75×10^{-2}	Maximum recruitment rate related to the PRW law	(6)
$g(nl)$		3.75×10^{-2}		(6)
$g(ln)$		1.13×10^{-1}		(6)

Table 2 continued

Parameter	Units	Value	Description	Source
$g(ll)$		3.00×10^{-1}		(6)
h	cell^2	2.02×10^7	Steepness coefficient for the recruitment related to the PRW law	(10)
a_{31}	cell $^{-1}$ day $^{-1}$	2.8×10^{-9}	Immune–tumor competition	(10)

The parameters of the PRW law, λ and d, are obtained by a least-squares fitting of the solutions of the system of differential equations to the experimental data. The parenthesis again represents four different cases: a primary challenge with control-transduced cells followed by a secondary one with ligand (*nl*) or control (*nn*) cells, and a primary interaction with ligand-transduced cells followed again by ligand (*ll*) or ligand-negative (*ln*) rechallenges

take the values of a_{13} used in such work and modify them the least as possible to obtain curves that resemble the ones shown there. The same procedure is followed for the steepness s of the saturation term in the PRW law. Then, the curves are fitted using the parameters d and λ. Trajectories are runned up to a maximum time of 4 h $t_{max} = 0.167$ days, at which the lysis of tumor cells $1 - T/T_0$ is measured in the experiments. Initial conditions are chosen to guarantee that the experimental effector:target ratios E_0/T_0 belong to the computed interval. The lysis of the tumor cells is obtained at t_{max} for the various initial conditions, and optimization is achieved by the least-squares method using a grid of values for the two parameters. The fitted curves for the model and its simplified version are shown in Fig. 2, while the residuals are depicted in Fig. 3. The general model fits the data nicely, with randomly distributed residuals. As expected, the reduced version gives worse results, specially for the control-transduced cells. The first four points in Fig. 2a, b can be fitted with exactness, but not the last one. Hence, a combination of a nonsaturating law with the PRW law gives considerably better results for the cases in which the immune response is less effective. These results suggest extending the PRW law by considering a fractional cell kill $F(E, T)$ given by the sum of a power law function and a Hill function

$$F(E, T) = cE^{\nu} + d\frac{E^{\lambda}}{h(T) + E^{\lambda}}. \tag{7}$$

Two limits can be clearly distinguished in this law. On the one hand, we have the situation in which the immune response is more or less effective $c \approx 0$, as shown in Fig. 2c, d. On the other hand, an ineffective immune response is given by $d \approx 0$, which corresponds to the NK cell lysis in De Pillis et al. (2005). Intermediate situations are better represented by (7), as shown in Fig. 2a, b. An heuristic explanation as to why less effective cells do not show saturation in practice can be given as follows. Suppose that we have two identical tumors of size T in the presence of the same number of effector cells, but the first E being very effective recognizing and lysing tumor cells, while the second $\tilde{E}$ being ineffective. The difference between these two cell populations can be represented by considering that in the second case, only a small fraction f of the effector cells are interacting with the tumor $\tilde{E} = fE$. Therefore, the PRW law becomes

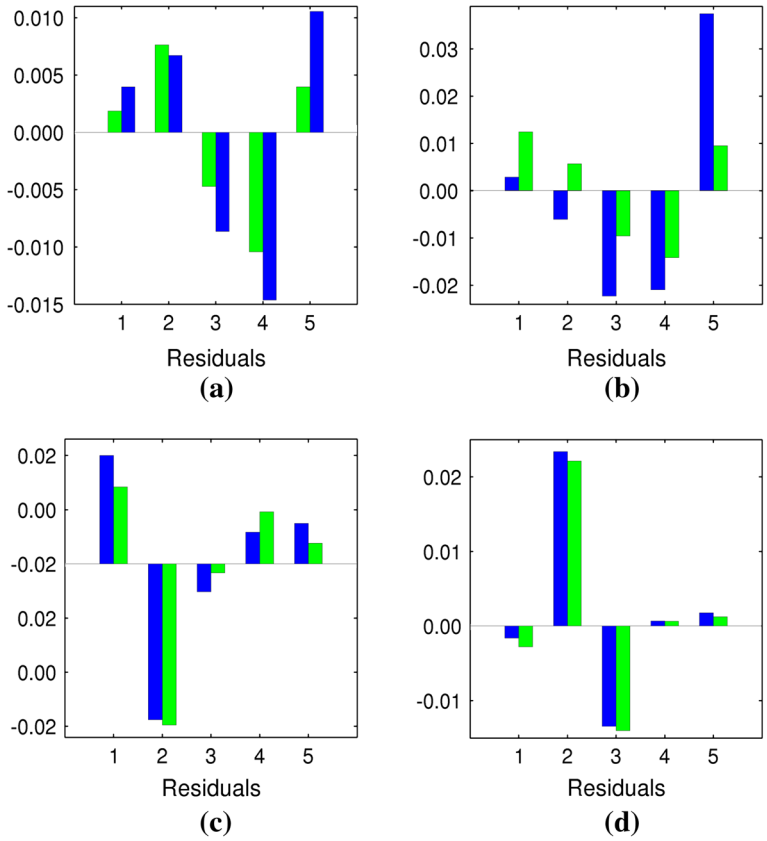

Fig. 3 Differences between the experimental data and the model estimated values (residuals) obtained from the predicted curves for the lysis of tumor cells by effector cells. The *green bars* correspond to the general model, while the *blue bars* belong to its simplified version. They are more or less randomly distributed. **a** The (nn) case represented in Fig. 2a. **b** The (nl) case represented in Fig. 2b. **c** The (ln) case represented in Fig. 2c. **d** The (ll) case represented in Fig. 2d (Color figure online)

$$D(\tilde{E}, T) = d\frac{f^{\lambda}E^{\lambda}}{h(T) + f^{\lambda}E^{\lambda}} = d\frac{E^{\lambda}}{\tilde{h}(T) + E^{\lambda}}, \tag{8}$$

where $\tilde{h}(T) = h(T)/f^{\lambda}$. In the case $f \ll 1$, and as long as E is not much higher than T, we get $\tilde{h}(T) \gg E^{\lambda}$, what yields the fractional cell kill $D(E, T) = E^{\lambda}/\tilde{h}(T)$. If the variation of T is small or $h(T)$ varies slowly with T, then the approximation cE^{λ} holds. For example, if we consider the parameter values of the (ll) experiment in Table 1 and take $f = 10^{-4}$, then we get a value for $\tilde{h}(T)$ two or three orders of magnitude higher than E^{λ}, depending on the values of the effector:target ratio.

4 Parameter and Phase Space Analysis

Even though the simplified model fits better the experiments where cells are primary challenged with ligand-transduced cells, to study the dynamics we concentrate on the

control-transduced choice of parameters. The reason is that the cell lines used in the experiments do not normally express ligands of the NKG2D receptor (Diefenbach et al. 2001). We begin by nondimensionalizing (5), redefining the cell populations and the time

$$\tilde{T} = \frac{T}{K_1}, \quad \tilde{H} = \frac{H}{K_2}, \quad \tilde{E} = \frac{r_1 E}{\sigma}, \quad \tilde{t} = t r_1. \tag{9}$$

The new parameters are related to the previous ones in the following way

$$\begin{aligned} \tilde{a}_{12} &= \frac{a_{12} K_2}{r_1} \quad \tilde{d} = \frac{d}{r_1} \quad \tilde{s} = s \left(\frac{K_1 r_1}{\sigma} \right)^{\lambda} \\ \tilde{r}_2 &= \frac{r_2}{r_1} \quad \tilde{a}_{21} = \frac{a_{21} K_1}{r_1} \\ \tilde{d}_3 &= \frac{d_3}{r_1} \quad \tilde{a}_{31} = \frac{a_{31} K_1}{r_1} \quad \tilde{g} = \frac{g}{r_1} \quad \tilde{h} = \frac{h}{(K_1 r_1)^2}. \end{aligned} \tag{10}$$

Dropping the tildes, our nondimensionalized system becomes

$$\begin{aligned} \dot{x} &= x(1-x) - a_{12} y x - D(x,z)x \\ \dot{y} &= r_2 y (1-y) - a_{21} x y \\ \dot{z} &= 1 - d_3 z + g \frac{D^2(x,z)x^2}{h + D^2(x,z)x^2} z - a_{31} x z. \end{aligned} \tag{11}$$

The rescaled parameters are $a_{12} = 0.195, d = 5.0, \lambda = 0.21, s = 11.5, r_2 = 0.35, a_{21} = 0.954, d_3 = 0.112, g = 0.29, h = 7.95 \times 10^{-11}$ and $a_{31} = 5.25$. Unless specified, these parameters are used all along our study.

We now describe all the nullclines and equilibria for the current set of parameters. The fixed points of the system are given by $\dot{x} = \dot{y} = \dot{z} = 0$, which yields the system of equations

$$\begin{aligned} 0 &= x\,(1 - x - a_{12} y - D(x,z)) \\ 0 &= y\,(r_2 - r_2 y - a_{21} x) \\ 0 &= 1 - d_3 z + g \frac{D^2(x,z)x^2}{h + D^2(x,z)x^2} z - a_{31} x z. \end{aligned} \tag{12}$$

Nullclines can be read directly from (12). There is a total of five nullclines: the x–z and y–z planes, the surface S_1 represented by the implicit equation $1 - x - a_{12} y - D(x,z) = 0$, the plane Π given by $r_2 - r_2 y - a_{21} x = 0$ and the surface S_2, which implicit equation is given by the last of the three equations shown above. If we restrict our attention to the biologically meaningful region, which is the positive octant $\mathbb{R}^+ \times \mathbb{R}^+ \times \mathbb{R}^+$, the intersections of the different nullclines yield five different fixed points x_i^*, as shown in Fig. 4. We give the numerical values of the fixed points and also analyze their stability by examining the eigenvalues of the Jacobian at each of them.

The first fixed point is $x_1^* = (0, 0, d_3^{-1})$, in particular $(0, 0, 8.93)$, a saddle with two positive eigenvalues corresponding to the x-axis and the y-axis, and a negative

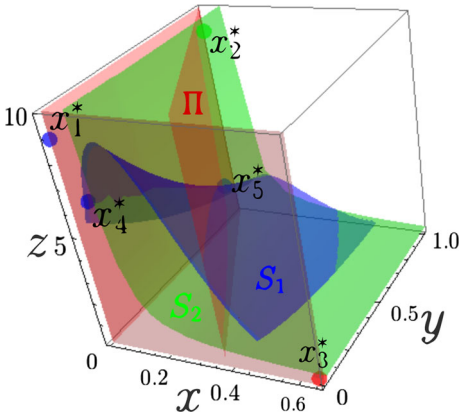

Fig. 4 Positive octant of the phase space with the nullclines and the fixed points. The surfaces represent the different nullclines, with the fixed points placed at some of their intersections. Every fixed point is the intersection of three surfaces. The surface S_2 has not been plotted completely for clarity, but it also intersects the y–z plane. The *green point* is the healthy state, while the *red point* is the tumor stable fixed point. The other three fixed points are saddles (Color figure online)

eigenvalue along the z-axis. The point $x_2^* = (0, 1, 8.93)$ represents the healthy state, for which there are only healthy and immune cells. Therefore, we represent it in green color. This fixed point is stable, being one of the attractors of the dynamical system. The other stable fixed point is $x_3^* = (0.65, 0, 0.31)$, representing a stable solution for which there are only tumor and immune cells. As in previous works (Gatenby and Gawlinsky 1996), we associate this fixed point to malignant growth, so we have colored it in red. The fixed point $x_4^* = (0.06, 0, 6.55)$ is a saddle fixed point with two unstable and one stable directions, separating the stable tumor attractor and the state x_1^*, which is attractive in such plane, and for which there are only immune cells. A stable direction and an unstable direction are in the plane $y = 0$, while the remaining unstable direction is given by the eigenvector $(0.01, 0.08, 1)$. The last fixed point is $x_5^* = (0.1, 0.74, 3.02)$, corresponding to the saddle fixed point, which two-dimensional stable manifold separates the basins of attraction of the healthy and the tumor stable states. Hence, the system is bistable. The evolution of the three cell populations for an initial condition leading to the malignant tumor state is shown in Fig. 5d.

We begin the parameter analysis studying the effects of varying d that affects the intensity with which the immune system destroys cancer cells. In Fig. 5a, b, we depict the change in the basins size due to increasing such parameter to a value of $d = 6.5$, while in Fig. 6a, a bifurcation diagram is computed, showing the evolution of the fixed points as such parameter is varied. Starting from high values of d, for which there is only a healthy stable state and the fixed point x_1^*, the parameter reaches a critical value of $d_c = 7.4185$ and a saddle-node bifurcation occurs. Another similar bifurcation appears for $d_c = 7.4095$. In total, four fixed points are born: three unstable and one stable. Only two of them are in the positive octant, the tumor fixed point x_3^* and x_4^*, both unstable. As we keep on decreasing the immune strength, for a value of $d_c = 7.2650$, the stable fixed point enters the positive octant and a transcritical bifurcation occurs, through which the malignant state switches its stability with the stable fixed point. These results are in agreement with Diefenbach et al. (2001), where cells that express ligands reject tumors, while control cells do not. The existence of a critical value d_c beyond which there is not a malignant tumor attractor constitutes an

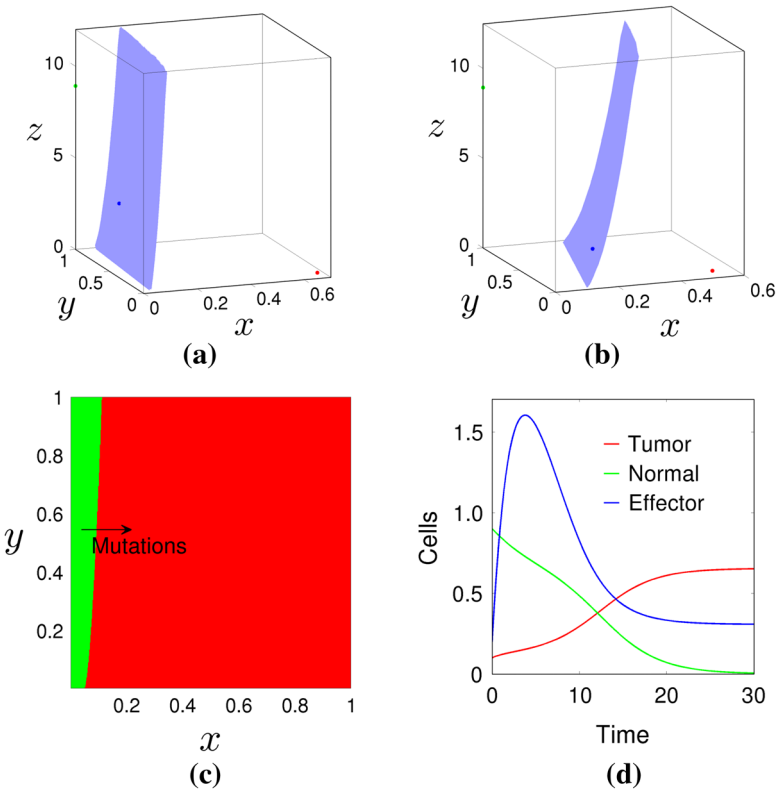

Fig. 5 **a** Stable manifold of the fixed point x_5^* (*blue*) separating the basins of attraction of the healthy x_2^* (*green*) and the tumor x_3^* (*red*) stable fixed points for $d = 5.0$. **b** Same figure but for $d = 6.5$. As the immune system response is stronger, the healthy basin enlarges and the tumor coordinate of the malignant attractor becomes smaller. **c** A section of the basins of attraction for $z = 3.5$. Oncogenic mutations can be understood as a crossing from the *green basin* to the *red* one. **d** Time series with the evolution of the three cell populations (nondimensional variables). As the tumor starts growing and replacing the normal tissue, the immune system orchestrates his response, activating the effector cells to counteract the proliferation of tumor cells. However, the effort is insufficient (Color figure online)

important prediction of the model, and might be used to estimate the minimum level of ligands required to ensure tumor regression through ligands expression. Also the parameter s is important in the model. Its behavior is opposed to the previous. As it is decreased, for a value of $s_c = 7.55$, a transcritical bifurcation occurs, turning unstable the malignant attractor. It again disappears through a saddle-node bifurcation for the critical value $s_c = 7.35$. However, the parameter λ does not change the stability of our dynamical system after considerable variations (even twenty times), although its increase leads to more negative eigenvalues of the tumor attractor, making this fixed point more attractive.

Looking at the basin of attraction in Fig. 5c, it might result surprising that a healthy state is always stably preserved. The reason is that cancer is the result of accumulated mutations and no mutations between healthy and cancerous phenotypes have been considered in the present model. This is in accordance, but also in contrast, with a

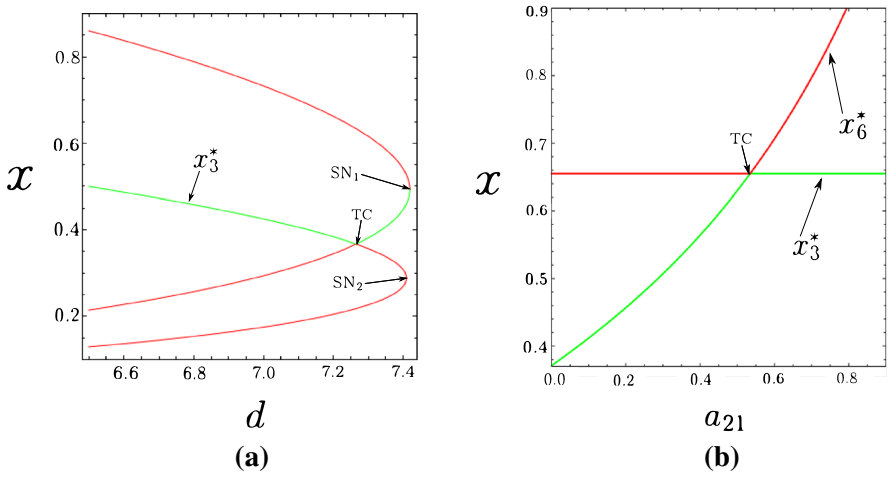

Fig. 6 **a** Bifurcation diagram for the tumor coordinate as we vary the parameter d, associated with the maximum fraction cell kill of the effector cells. As such parameter is decreased from values $d > 7.4$, for which there is only a healthy state, two saddle-node (SN_1 and SN_2) bifurcations occur, giving birth to four fixed points, among which figures the tumor one, still unstable. Later on, a transcritical bifurcation (TC) turns the tumor stable fixed point x_3^* stable, by switching stability with another fixed point. The stable attractor is shown in green, while the unstable saddles are painted in *red*. **b** The bifurcation diagram for the tumor coordinate as we vary the parameter a_{21}. For high values of a_{21}, the fixed point x_6^*, corresponding to an equilibria for which all the cell populations coexist, is unstable and placed out of the positive octant. As we decrease a_{21}, it enters the positive octant and switches stability with the malignant tumor fixed point x_3^* through a transcritical bifurcation (TC). The tumor shrinks as we keep on decreasing the value of a_{21} (Color figure online)

simple logistic growth model, for which the zero value of the tumor cell population is a fixed point, but it is unstable, so that any small perturbation pulls the dynamics away from it. The homologous to such zero cell population fixed point in the present model is x_1^*, which is always unstable. However, as we argue in detail in the next paragraph, a healthy stable state will be preserved unless the action of the immune system and the competition of the healthy cells with the cancer cells are negligible, what is in consonance with the fact that apoptosis is a major barrier to tumor growth that must be circumvented (Hanahan and Weinberg 2000). The effect of mutations can be associated with a passage from one basin to the other. The smaller the basin of attraction of the healthy point is, the easier for a tumor to be born. Mutations can be modeled in several manners, for example, considering multiplicative noises on some parameters of the model, or introducing balanced decay and growth terms in the host and the tumor cell differential equations, respectively (Ideta et al. 2008; Gardner 2002), like in the quasispecies formalism (Nowak 1992).

Concerning the tumor–host competition terms a_{12} and a_{21}, the following behavior is observed. In an ordinary Lotka–Volterra competition model with two populations (N_1, N_2) (no immune response), the stability of the fixed point $(0, K_2)$ depends upon the competition term a_{12} affecting the other population, and vice versa. In such a model, if $a_{12} > r_1/K_2$, then the fixed point $(0, K_2)$ is stable, while if it is smaller, the point becomes unstable. The immune system introduces an innovation in this scenario as long as d is not very small, since no matter how small a_{12} is made, the

effector cells are killing tumor cells, what means that there is always a healthy state. On the other hand, if we decrease the parameter a_{21} more than the critical value 0.535, a transcritical bifurcation occurs for which the tumor fixed point x_3^* becomes unstable and a equilibria x_6^* representing the coexistence of the three species arises in the positive octant, becoming stable. As can be seen in Fig. 6b, for $a_{21} = 0.5$, such equilibria are $x_6^* = (0.63, 0.10, 0.32)$. A big tumor coexists with the healthy tissue. As we keep on decreasing the value of a_{21}, the tumor shrinks and the healthy tissue swells, what corresponds to a more benignant state. Thus, the maximum size a tumor can reach according to our model, depends noticeably on its capability to reduce the host healthy cells living with it, which in part is related to aerobic glycolysis.

5 Fitting the Chemotherapy Treatment to Experiments

Therapies are the main practical reason for studying tumor growth. Two important restrictions in the application of chemotherapy are the toxicity of the drugs and the resistance of tumor cells to such cytotoxic agents. In order to properly model and understand these two processes in our context, a realistic modeling of chemotherapy must be attained in the first place. Depending on their particular mechanism of action (alkylation, topoisomerase inhibition, antimetabolism, etc.), cytotoxic chemotherapeutic agents can be classified into two main groups: cell cycle specific (CS) and non-specific (CNS). Both types of drugs appear commonly combined in many therapies. For example, locally advanced breast cancer uses cyclophosphamide, doxorubicin and docetaxel. Therefore, we shall utilize a model capable of reproducing CS and CNS drugs, preferably not requiring explicit modeling through several cell populations in different stages of the cell cycle, as in other works (Panetta and Adam 1995). A mechanistic model that has been tested with in vitro experiments for both types of drugs is the exponential kill model. This model has been already used (De Pillis et al. 2005; Gardner 2002; De Pillis et al. 2006) and proposes a fractional cell kill law of the form

$$k(C) = b(1 - e^{-\rho C}), \tag{13}$$

where C is the drug concentration at the tumor site, and for CS drugs, b depends on the fraction of cells in a vulnerable part of the cell cycle at a certain time instant, and the cells rate of entry and abandon of such phase of the cycle. In the case of CNS drugs, such parameter is equal to one. The scaling parameter ρ is related to the levels of drug resistance. This factional cell kill law means that for a given dose of drug, after a certain period of time, the tumor is reduced to a particular fraction of its size, no matter how big or small it was initially (Hiramoto and Ghanta 1974). Survival fractions can be analytically obtained assuming exponential growth and constant concentrations of the drug (Gardner 1996), but neither of these two situations generally hold for in vivo experiments. We have modified this law, so that it depends on the time-delayed concentration. This is the simplest modification we have been able to elucidate that permits to fit the data. The significance of this method will be discussed ahead. In this first approach, to fit the experiments, we neglect the cytotoxic effects of the drug on the healthy tissue. The resulting nonautonomous dynamical system reads

$$\begin{aligned}\dot{x} &= x(1-x) - a_{12}yx - D(x,z)x - b(1-e^{-\rho u(t-\tau)})x\\ \dot{y} &= r_2 y(1-y) - a_{21}xy\\ \dot{z} &= 1 - d_3 z + g\frac{D^2(x,z)x^2}{h + D^2(x,z)x^2}z - a_{31}xz,\end{aligned} \tag{14}$$

with $u(t) = u_0 e^{-k_e t}$ for $t \geq 0$ and zero if $t < 0$. Hence, a single dose of drug is administered at $t = 0$, but it starts to cause its effect at time τ. The relations between the chemotherapy parameters of the nondimensional model and the originals shown in (6) are as follows

$$\tilde{b} = \frac{b}{r_1} \quad \tilde{\tau} = \tau r_1 \quad \tilde{k_e} = \frac{k_e}{r_1}, \tag{15}$$

where tildes have been excluded again in (14).

The data used to fix the parameters of the chemotherapy treatment are borrowed from Hiramoto and Ghanta (1974). In this study, a plasmacytome is inoculated into BALB/c mice and allowed to grow up to a certain size. Then, the animals receive cyclophosphamide, a cell cycle nonspecific alkylating agent, and tumor regression is observed days later. To validate the modeled chemotherapy treatment, we use the results from two experiments. In the first one, five mice are given subcutaneous injections of 1×10^3 viable MOPC 104E cells, and the tumor is allowed to grow up to 0.09 g (1 g equals 1×10^9 tumor cells). Cyclophosphamide is given at a single dose after palpable nodules are present. In the second experiment, three mice receive intravenous injections of 1×10^6 cells of the same cell line, and the tumor is allowed to proliferate up to maximum size of 2.90 g. They use three mice as control with mescaline treatment and three more with a single dose of cyclophosphamide. They are able to estimate the size of the tumor from the immunoglobuline M levels using a linear model $\dot{M} = T - kM$, being M the IgM levels and T the tumor size, which is assumed to grow exponentially $T(t) = T_0 e^{\alpha t}$, with α a function of the doubling time of tumor cells. The parameter k represents the removal rate of IgM from circulation. The dose of drug administered in the experiments is 200 mg/kg, and the mice weight around 20 g, so we take $u_0 = 4$ mg. We consider that the drug elimination rate is $k_e = 2.5$ day^{-1}, what approximately corresponds to a half-life of 6.5 h. In the first experiment in Hiramoto and Ghanta (1974), the averages of the tumor weight and the mass percentage of the tumor respect to the total mass are reported. In the second experiment, the same magnitudes are addressed for each of the three mice. We limit ourselves to the first mouse results, which tumor grows bigger. Because no data concerning the tumor–immune interaction are provided in these two experiments, we cannot properly fit the model given by (5). For this reason, we use the nondimensional model with the parameter values given in Sect. 4, and the mass percentage of the tumor measured in the experiments, and set the initial conditions (x_0, y_0, z_0) proceeding as follows. In the first experiment, the therapy begins at day 22, when the tumor size reaches the 4 % of the total body weight. Therefore, we consider that the x coordinate of the fixed point associated with the malignant tumor state x_3^*, represents a size of 5 % of the total body, i.e., $x_0 = x_3^* \times 0.4/0.5$. An identical prescription is followed with the second experiment, for which the tumor reaches a size of 12 % of the total body weight. Now we make $x_0 = x_3^* \times 12/15$. Since in the second experiment, large

Table 3 Values of the level of drug resistance and the time it takes the drug to start causing its cytotoxic effect

Parameter	Units	Value	Description
Experiment 1			
ρ	mg^{-1}	4.04×10^3	Level of drug resistance
τ	day	4.18	Time delay
Experiment 2			
ρ	mg^{-1}	4.03×10^3	Level of drug resistance
τ	day	3.56	Time delay

They are obtained through a least-squares fitting of the solutions of (14) to two different experimental situations were mice are treated with cyclophosphamide

implants of intravenously disseminated tumors are studied, while the first experiment deals with small localized subcutaneous tumors, we consider different initial conditions concerning the effector cells for each experiment, assuming that in the second one the immune response is stronger. In particular, the values we use are, respectively, $z_0 = 7.0$ and $z_0 = 1.0$. The initial condition for the healthy tissue is taken $y_0 = 0.5$ in both experiments. These initial conditions lead to the tumor stable fixed point in the absence of treatment, and other choices might be used as well. The parameter values τ and ρ arranged to fit the fractional tumor cell kill by cyclophosphamide are obtained following the same method as in Sect. 3. We show them in Table 3 for both cases. The time delay is longer in the first experiment, probably because small localized tumors are harder to reach than large implants. The levels of drug resistance are certainly low (high values of ρ), and similar for the two experiments.

In Figs. 7 and 8, we can see that the model validates well the experimental results. During the first three/four days, the drug has little effect on the tumor, and from this day on, a severe decrease is observed. Along these first days, we recognize that the curves are slightly concave and then rise up, before cyclophosphamide starts to be effective. This is a consequence of the immune system, that is, destroying proliferating tumor cells. After this first period of time, the drug starts to cause its effect and dominates the dynamics during the next five/six days. From this day on, the immune system takes care of the remaining part of the tumor and the healthy tissue regenerates. The action of chemotherapy can be thought as a passage from the red basin to the green one in Fig. 5c. We believe that the lag in the action of the drug is due to complex pharmacokinetics. In general, it takes a time for the drugs to reach the tumor site and be absorbed, as well as to inflict damage to the proliferating cells through its cytotoxic mechanism. In particular, it might happen that different drugs have different time delays, what might play a role in modeling combination therapy when studying tumor resistance to chemotherapeutic agents, and also their toxicity.

The dynamical response to chemotherapy mainly consists in a change of the basin size. The higher the dose, the bigger the healthy basin. The manifold separating the basins of attraction moves to the right and rotates clockwise. The results are similar to those shown in Fig. 5a, b, and also in previous works (De Pillis and Radunskaya 2003), so we do not show them. It is important to recall that the nonautonomous system given by (14) tends to the original system asymptotically. This means that

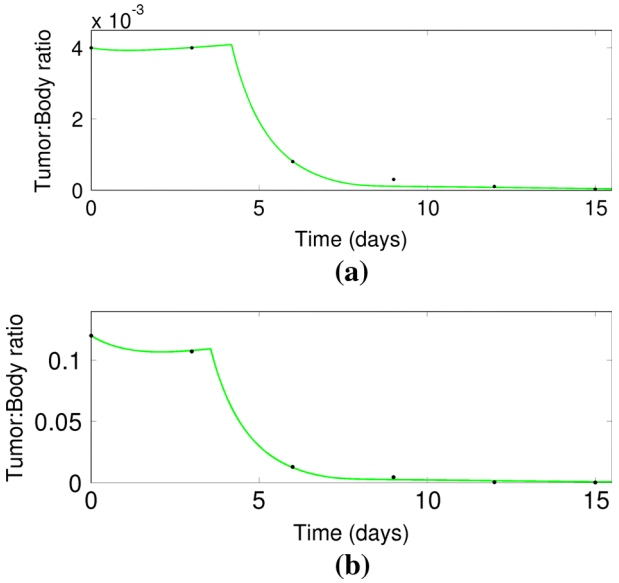

Fig. 7 **a** Data in the first experiment and the model predicted curve for the tumor decay after a single-dose injection of cyclophosphamide is delivered into the mice. The y-axis represents the fraction of tumor cells in the body. During the first days, the drug has little effect on the host, and then, the tumor cells are strongly reduced. **b** Data for the second experiment and the model predicted curve for the tumor decay after a single-dose injection of cyclophosphamide is delivered into the mice

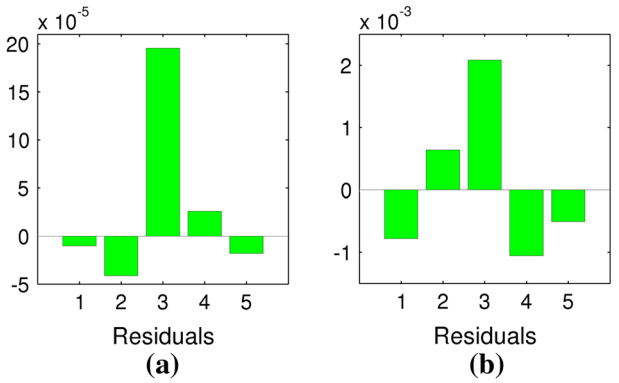

Fig. 8 **a** Residuals of the fitted data in the first experiment, corresponding to Fig. 7a. **b** Residuals of the fitted data in the second experiment, corresponding to Fig. 7b

although the basins structure and size change during the treatment, once the drugs are eliminated, the original dynamical system is restored, and so they are its stability properties. Consequently, a tumor relapse requiring to resume the chemotherapeutic treatment would be expected. On the other hand, as shown in Sect. 4, therapies implying a change in the parameter values of the dynamical system, as it is the purpose of immunotherapeutic vaccines (Diefenbach et al. 2001; De Pillis et al. 2006), are

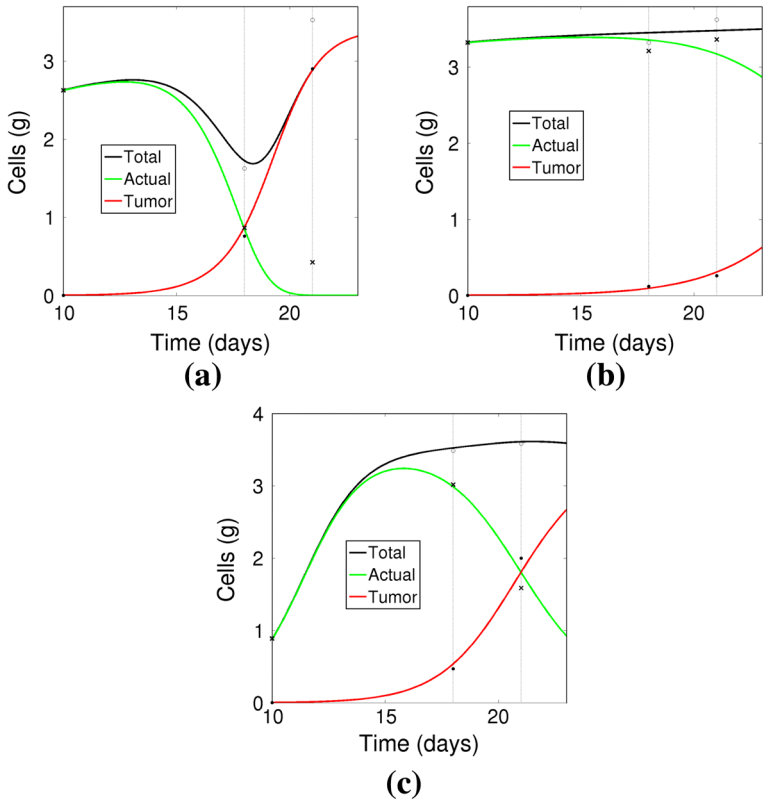

Fig. 9 Time series given by the model (*solid curves*) and the experimental data of the tumor (*filled circle*), the actual (*cross symbol*) and the total (*open circle*) cell populations for the three mice in the second experiment in Hiramoto and Ghanta (1974). The first points are used to fix initial conditions. **a** For the first animal, the actual and the total sizes first decrease because the healthy tissue is being destroyed. Then, the growth of the tumor rises and the total and the tumor cell populations become equal. **b** In the second animal, the tumor grows very slowly and the cell populations are almost constant. **c** In the third case, the healthy cells start to grow together with the tumor, but as the tumor increases the normal cells reach a peak and begin to die (Color figure online)

obviously more advantageous, because they can change the stability properties of the dynamical system permanently, preventing the disease from recurring.

6 Experimental Correlations with the Model

This section is devoted to expose some correlations between the model and the experimental data appearing in Hiramoto and Ghanta (1974), with the aim of obtaining rough estimations of the parameters a_{12} and a_{21}. In particular, the experimental results correspond to the same experiment as those shown in Fig. 7b, but now we focus on the growth of the tumor before therapy is applied. In that experiment, the actual body weight, which is defined as the difference between the total weight of each mouse and the weight of their respective tumors, is computed. For the cyclophosphamide-treated

Table 4 Values of the parameters in the simplified model that were required to change in order to describe the growth of the plasmacytome, the time evolution of the body weight and the time evolution of the actual body weight, for the three mice in the second experiment in Hiramoto and Ghanta (1974)

Parameter	Units	Value	Description
Mouse 1			
K_1	cells	3.4×10^9	Carrying capacity of tumor cells
K_2	cells	3.5×10^9	Carrying capacity of healthy cells
r_1	day^{-1}	0.95	Rate of growth of tumor cells
r_2	day^{-1}	0.06	Rate of growth of normal cells
a_{12}	$\text{cells}^{-1}\,\text{day}^{-1}$	4.8×10^{-11}	Competition of healthy cells with tumor cells
a_{21}	$\text{cells}^{-1}\,\text{day}^{-1}$	6.0×10^{-10}	Competition of tumor cells with healthy cells
Mouse 2			
K_1	cells	3.4×10^9	Carrying capacity of tumor cells
K_2	cells	3.5×10^9	Carrying capacity of healthy cells
r_1	day^{-1}	0.62	Rate of growth of tumor cells
r_2	day^{-1}	0.13	Rate of growth of normal cells
a_{12}	$\text{cells}^{-1}\,\text{day}^{-1}$	4.8×10^{-11}	Competition of healthy cells with tumor cells
a_{21}	$\text{cells}^{-1}\,\text{day}^{-1}$	1.3×10^{-10}	Competition of tumor cells with healthy cells
Mouse 3			
K_1	cells	3.4×10^9	Carrying capacity of tumor cells
K_2	cells	3.5×10^9	Carrying capacity of healthy cells
r_1	day^{-1}	0.82	Rate of growth of tumor cells
r_2	day^{-1}	0.49	Rate of growth of normal cells
a_{12}	$\text{cells}^{-1}\,\text{day}^{-1}$	3.7×10^{-11}	Competition of healthy cells with tumor cells
a_{21}	$\text{cells}^{-1}\,\text{day}^{-1}$	2.3×10^{-10}	Competition of tumor cells with healthy cells

group, the data are registered at days 10, 18 and 21, the last corresponding to the beginning of the treatment (see Fig. 9). It is hard to know whether these variations are due to differences in the tumor cells and the healthy cells interacting with them, consequence of other cells in the body, changes in the metabolism or, more simply, nourishment. Nevertheless, we believe that it is good to show that our model is compatible with such results, mainly to assure ourselves that the parameter values of the competition terms are biologically reasonable. For these reasons and because no data concerning the tumor–immune interaction are available in these experiments, we do not fit the curves.

We relate the total body weight to the sum of the three cell populations, while the actual body weight is considered to be the sum of the healthy and the immune cell populations. Since the last is considerably smaller than the former, the actual population of cells looks like the normal cells population. We also consider the approximation $d = 0$ (otherwise small tumor sizes lead to the healthy attractor), which is reasonable during the first days of tumor growth, since it takes the body some time to develop an immune response. The plots in Fig. 9 show similar behaviors of the experimental

data and the theoretical predicted values by the model at days 18 and 21 for the three mice. In some cases, the correspondence is not only qualitative, but also quantitative.

As we can see in Fig. 9, for the first mouse, there is a decrease of the healthy cell population, what implies a decrease of the actual and total populations at day 18. Later on, the tumor increases and the total population rises, while the healthy host cells keep on being destroyed. Interestingly, in this case, a better correlation between the experimental data and the theoretical predicted curves at day 21 can be achieved if saturation of the competition term given by a_{21} with the tumor load is considered. This saturation would be explained by the fact that competition for space occurs between nearby cells, and competition for nutrients occurs along the direction of the gradient of nutrient concentration. For the second mouse, the tumor grows very slowly, so the cell populations remain almost constant. In the third case, since the mouse has smaller weight, we choose a smaller value of the healthy cell population as an initial condition. The population starts to increase and so does the tumor. A maximum actual weight is observed at day 18, and then, the healthy cell population starts to decrease due to the growth of the tumor. However, the total weight at day 21 is almost the same, because the tumor has grown considerably. The parameters we have had to change from the ones settled in (5) to reproduce the experiments are shown in Table 4. Note that for every mouse, $a_{21} > a_{12}$ holds, as conjectured in Sect. 3.

7 Conclusions and Discussion

We have developed a model of tumor growth taking into account the heterogeneity of the tissue as a complex interaction between several types of cells. The model includes tumor–immune and tumor–host interactions, which are in conformity with experimental data. We have examined the dynamical properties of the model, showing its correlation with theoretical and empirical knowledge of tumor progression. Also chemotherapy has been studied, and a way to overcome the problem of modeling complex drug dynamics has been proposed. We believe that the model might be useful when attempting to embark the study of tumor growth. Of course, ODE-based modeling and the present model itself are both far away from being definitive. Rather, they might be used as a foundation upon which to build up different and increasingly more sophisticated models, capable of reproducing the many aspects of the tremendously complex dynamics of cancer inception and evolution at its different, but inextricably related, scales.

Acknowledgments This work was supported by the Spanish Ministry of Economy and Competitivity under Project Number FIS2013-40653-P.

References

Bellomo N, Li NK, Maini PK (2008) On the foundations of cancer modelling: selected topics, speculations, and perspectives. Math Models Methods Appl Sci 18:593–646

Couzin-Frankel J (2013) Cancer immunotherapy. Science 342:1432–1433

De Pillis LG, Radunskaya A (2003) The dynamics of an optimally controlled tumor model: a case study. Math Comput Model 37:1221–1244

De Pillis LG, Radunskaya AE, Wiseman CL (2005) A validated mathematical model of cell-mediated immune response to tumor growth. Cancer Res 65:235–252
De Pillis LG, Gu W, Radunskaya AE (2006) Mixed immunotherapy and chemotherapy of tumors: modelling, applications and biological interpretations. J Theor Biol 238:841–862
Diefenbach A, Jensen ER, Jamieson AM, Rauelt DG (2001) Rae1 and H60 ligands of the NKG2D receptor stimulate tumor immunity. Nature 413:165–171
Dudley ME, Wunderlich JR, Robbins PF, Yang JC, Hwu P, Schwartzentruber DJ, Topalian SL, Sherry R, Restifo NP, Hubicki AM, Robinson MR, Raffeld M, Duray P, Seipp CA, Rogers-Freezer L, Morton KE, Mavroukakis SA, White DE, Rosenberg SA (2002) Cancer regression and autoimmunity in patients after clonal repopulation with antitumor lymphocytes. Science 298:850854
Ferreira SC Jr, Martins ML, Vilela MJ (2002) Reaction-diffusion model for the growth of avascular tumor. Phys Rev E 67:051914
Gardner SN (1996) A mechanistic, predictive model of dose-response curves for cell cycle phase-specific and nonspecific drugs. Cancer Res 60:1417–1425
Gardner SM (2002) Modeling multi-drug chemotherapy: tailoring treatment to individuals. J Theor Biol 214:181–207
Gatenby RA, Gawlinsky ET (1996) A reaction–diffusion model of cancer invasion. Cancer Res 56:5475–5753
Hanahan D, Weinberg RA (2000) Hallmarks of cancer. Cell 100:5770
Hiramoto RN, Ghanta VK (1974) Chemotherapy and rate of kill of tumor cells in a mouse plasmacytome. Cancer Res 34:1738–1742
Ideta AM, Tanaka G, Takeuchi T, Aihara K (2008) A mathematical model of intermittent androgen suppression for prostate cancer. J Nonlinear Sci 18:593–614
Kirschner D, Panetta JC (1988) Modelling immunotherapy of the tumor–immune interaction. J Math Biol 37:235–252
Kuznetsov VA, Makalkin IA, Taylor MA, Perelson AS (1994) Nonlinear dynamics of immunogenic tumors: parameter estimation and global bifurcation analysis. Bull Math Biol 56:295321
Lavi O, Gottesman MM, Levy D (2012) The dynamics of drug resistance: a mathematical perspective. Drug Resist Updat 15:90–97
Mallet DG, De Pillis LG (2006) A cellular automata model of tumor–immune system interactions. J Theor Biol 239:334–350
Nowak MA (1992) What is quasispecies? Trends Ecol Evol 7:118–121
Olumi AF, Gary DG, Hayward SW, Carrol PR, Tlsty RD, Cunha GR (1999) Carcinoma-associated fibroblasts direct tumor progression of initiated human prostatic epithelium. Cancer Res 59:5002–5011
Panetta JC, Adam J (1995) A mathematical model of cycle-specific chemotherapy. Math Comput Model 22:67–82
Pastorino F, Brignole C, Di Paolo D, Nico B, Pezzolo A, Marimpietri D, Pagnan G, Piccardi F, Cilli M, Longhi R, Ribatti D, Corti A, Allen MT, Ponzoni M (2006) Targeting liposomal chemotherapy via both tumor cell-specific and tumor vasculature-specific ligands potentiates therapeutic efficacy. Cancer Res 66:10073–10082
Pinho STP, Freedman HI, Nani F (2002) A chemotherapy model for the treatment of cancer with metastasis. Math Comput Model 36:773–803
Van der Heiden MG, Cantley LC, Thompson CB (2009) Understanding the Warburg effect: the metabolic requirements of cell proliferation. Science 324:1029–1033
Warburg O (1956) On the origin of cancer cells. Science 123:309–314